Experimental and Computational Study of a Swept Compression Corner Interaction Flowfield

G. S. Settles*
Pennsylvania State University, University Park, Pennsylvania
C. C. Horstman†
NASA Ames Research Center, Moffett Field, California
and
T. M. McKenzie‡
Princeton University, Princeton, New Jersey

The results of an experimental and computational study of the three-dimensional shock-wave/turbulent boundary-layer interaction generated by a swept compression corner are presented. This corner had a streamwise compression angle of 24 deg and a sweepback angle of 40 deg. Two equilibrium incoming turbulent boundary layers with thicknesses varying by 3:1 were used. In both cases the freestream Mach number was 2.95, the freestream Reynolds number was 63×10^6/m, and the wall temperature was close to adiabatic. This study was undertaken to test the applicability to flowfield features of a Reynolds number similarity law originally based on surface features only. A second goal of the study was to test the ability of a state-of-the-art numerical solution of the Navier-Stokes equations to predict the subject flow. The experimental results, composed primarily of flowfield pitot pressure and yaw angle surveys, confirmed the general applicability of the similarity law. The comparison of experiment and computation revealed that the latter captured may of the qualitative features of the flow. Further, only very limited reasons were found to prefer a two-equation eddy-viscosity turbulence model rather than an algebraic model for predictions of this flow.

Nomenclature

a = exponent in Re_δ similarity law
c_f = skin-friction coefficient
L_M = upstream influence distance ahead of corner in x direction
M = Mach number
p = static pressure
Re_{δ_0} = Reynolds number based on incoming boundary-layer thickness
T = temperature
u,v,w = velocity components in x,y,z directions, respectively
x,y,z = orthogonal coordinate system (see Fig. 1)
α = compression corner angle of attack in x-y plane
δ = boundary-layer thickness
δ^* = boundary-layer displacement thickness
θ = boundary-layer momentum thickness
λ = compression corner sweepback angle in x-z plane
μ = molecular viscosity
Π = boundary-layer wake strength parameter
ρ = density
τ = shear stress

Subscripts

A = apex of corner model
C = corner
f = floor
p = plate
R = reattachment line
S = separation line
t = stagnation
u = unit
w = wall
0 = incoming condition
∞ = freestream

Presented as Paper 84-0096 at the AIAA 22nd Aerospace Sciences Meeting, Reno, NV, Jan. 9-12, 1984; received Jan. 24, 1984; revision received July 16, 1985.

*Associate Professor, Mechanical Engineering Department. Member AIAA.
†Assistant Chief, Experimental Fluid Dynamics Branch. Associate Fellow AIAA.
‡Graduate Student, Gas Dynamics Laboratory.

Introduction

PROBLEMS of three-dimensional (3D) shock-wave/turbulent boundary-layer interactions are both practically significant and dauntingly complex. Until recently, very little was known about these problems. There has been some important progress toward their understanding over the past decade (see, for example, Refs. 1-7), but the problems are by no means solved. The recent progress in large-scale numerical solutions of complex flows has permitted attempts at predicting 3D interactions,[7-12] but again no truly accurate and general predictions have been made.

The approach of the computational predictors has been to solve the Reynolds-averaged Navier-Stokes equations for interaction geometries which have undergone experimental study. The approach of the experimentalists has usually been to study interactions that are relatively "simple," at least as far as the inviscid flowfield is concerned. This approach is based on the rationale that a physical understanding of basic flows hopefully can be used to analyze more complex flows.

The most-often-studied "basic" 3D shock/boundary-layer interaction is that generated by a planar swept normal shock wave from a sharp fin at angle of attack.[1,2,5-8,12] While much has been learned from these studies, this type of interaction is inherently restricted to high sweepback angles. Efforts to explore the full range of interaction sweepback and shock strength have thus required different shock generator geometries, chief among which is the swept compression corner.

Swept corners can produce a range of 3D shock/boundary-layer interactions extending from the two-dimensional (2D) limit up to the highly swept cases produced by fins. A series of parametric swept corner experiments has recently been carried out to explore the interaction regimes and

physical mechanisms over this entire range at Mach 3.[2-4,10,13-17] Briefly, two distinct flow regimes were found: quasicylindrical and quasiconical.[4] The boundary between these regimes corresponds to inviscid shock detachment from the swept corner. Within the cylindrical regime a modified form of the classical independence principle holds,[15] while within the conical regime a similarity law has been found relating the interaction character to the structure of the imposed inviscid flow.[5,16]

The studies described above were restricted to semi-infinite swept corner shock generators which imposed no significant dimension upon the interaction development. In such cases the dimensional scales of the interaction must depend upon the incoming 2D turbulent boundary layer, which possesses the only independent linear dimension in the problem. Settles and Bogdonoff[3] formulated an interaction similarity law in terms of the boundary-layer thickness Reynolds number to describe this phenomenon:

$$(x_w/\delta_0)Re_{\delta_0}^a = f[(z_w/\delta_0)Re_{\delta_0}^a] \qquad (\alpha,\lambda,M_\infty \text{ fixed}) \qquad (1)$$

where the left-hand term and the argument of the function are nondimensional forms of the x and z interaction coordinates, respectively. The empirical exponent "a" in Eq. (1) falls between 0.3 and 0.4 for a freestream Mach number of 3 for both 2D and 3D compression corners, and is a weak function (not usually considered) of the corner defining angles.

Since the Reynolds number effect given by Eq. (1) is uniform in both the x and z directions, the interaction *shape* is unaffected by Reynolds number changes and geometrical similarity is preserved:

$$x_w/z_w = f(\alpha,\lambda,M_\infty) \qquad (2)$$

Note, however, that this similarity law was initially verified only for the interaction "footprint" (i.e., $y=0$).

Flowfield survey measurements are required to check the similarity law off the interaction surface. Such surveys were made in Ref. 6 for the case of a fin-generated interaction. The results showed that Eq. (1) was successful in scaling the interaction flowfield as well as the footprint.

The purpose of the present study is to explore the flowfield structure of a swept compression corner interaction and to perform a similar test of Eq. (1) in that context. Further, the experimental data are compared with the predictions of a state-of-the-art numerical solution of the Navier-Stokes equations. To the authors' knowledge, this represents the first Navier-Stokes solution of a swept corner interaction.

Description of Experiments

The rather extensive experimental program upon which this paper is based is fully described in Ref. 17. The present description is thus appropriately abbreviated.

Wind Tunnel

The experiments were carried out in the Princeton University 20×20 cm supersonic wind tunnel. The stagnation pressure and temperature were 0.69×10^6 N/m^2 ±1% and 260 K ±4%, respectively, giving a freestream Reynolds number of 63×10^6/m ±5%. The freestream Mach number was 2.95. All tests were conducted with near-adiabatic wall conditions ($T_w/T_t=1.03$).

Test Configurations

A swept compression corner defined by a streamwise angle of 24 deg and a sweepback angle of 40 deg was chosen as the test case. As shown in Fig. 1, this model was tested both on the wind-tunnel floor and on a flat plate with a sharp leading edge which spanned the wind tunnel. The 15.24-cm width of the model allowed it to be isolated from the tunnel sidewall

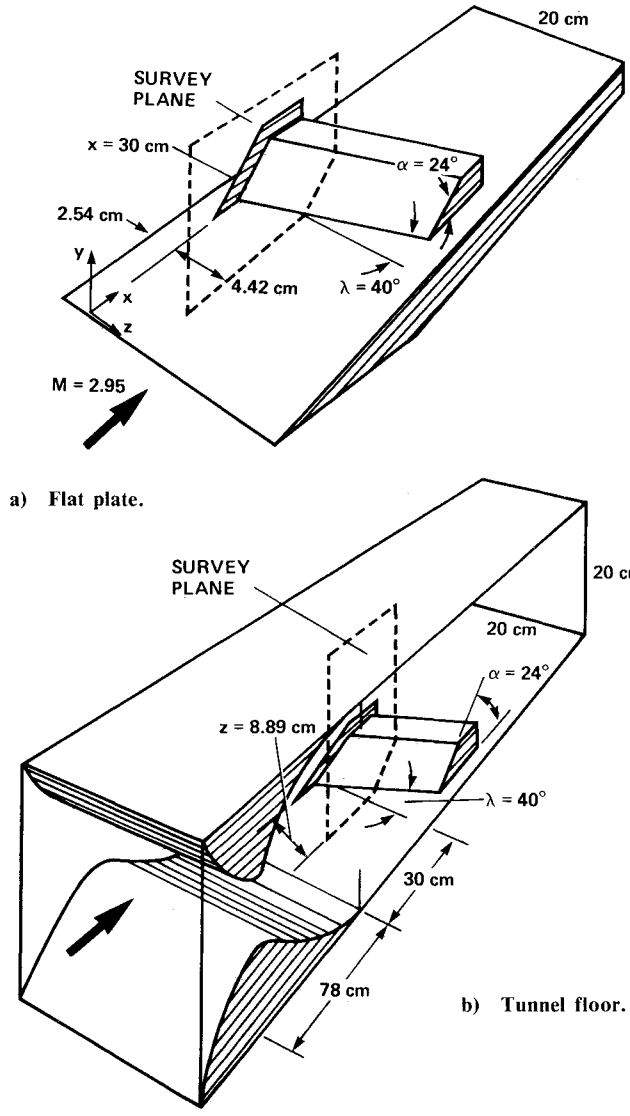

Fig. 1 Swept corner configurations.

boundary layers. An aerodynamic fence on the upstream model side also aided this purpose. For the tunnel-floor installation there were four streamwise surface pressure tap rows located at $z=5.08$, 7.62, 10.16, and 12.70 cm, while the plate had three tap rows at $z=0.41$, 4.22, and 6.12 cm.

Measurement Techniques

Surface Properties

Surface pressure readings were taken at the above-indicated tap row locations using a computer-controlled Scanivalve system. Detailed surface streak patterns were obtained by way of an adaptation of the kerosene-lampblack technique.[14]

Flowfield Properties

A computer-controlled autonulling yaw probe was used to measure pitot pressure and flow angularity in the x-y survey planes indicated in Fig. 1. Upstream of the corner the probe traversed normal to the floor and plate surfaces (i.e., along vertical lines) and rotated in planes parallel to those surfaces, with the probe tip remaining on the axis of rotation. From the corner location to a position 2.5 cm downstream on the model surface, surveys were made along lines tilted 16 deg forward of the vertical direction. Downstream of this position the survey lines were tilted 24 deg forward of the vertical. The zero-yaw reference was taken to be the undisturbed freestream flow direction in all cases.

The yaw probe tip consisted of three orifices; the center orifice was normal to the flow while those at either side were cut back at 45-deg angles. The overall tip dimensions were 0.06-cm high by 0.33-cm wide. The center orifice, used to measure pitot pressure, was connected to a miniature pressure transducer located inside the probe shaft. The outer orifices were connected across a similar transducer of the differential type. The output of the latter was used to indicate probe misalignment with the local flow, and was part of a feedback loop which rotated the probe tip to a null position under computer control.

Extensive tests were carried out to evaluate possible probe interference with the flow.[17] Some local interference was detected with the probe tip in the immediate vicinity of the test surface, but these conditions represented a small fraction of the total survey program. No global interference (i.e., gross alteration of the flow) was detected. The overall accuracy of measured yaw angle was estimated to be $\pm 1\%$, and that of probe tip placement ± 0.02 cm in x and y. The repeatability of the data was generally within $\pm 1\%$.

Incoming Boundary Layers

The incoming turbulent boundary layers on both the plate and the tunnel floor have been surveyed extensively. Both are equilibrium layers which agree with the standard compressible wall-wake similarity law.[17,18] The incoming boundary-layer parameter values are given in Table 1. The computed values were matched for δ_0^* and were within $\pm 15\%$ for the other parameters shown in the table.

Survey Locations

As described previously, it was desired to carry out flowfield surveys in both the floor and plate interactions at comparable spanwise locations in order to check the Reynolds number similarity law [Eq. (1)]. This required that the x-y survey planes be at different physical distances z from the swept corner apex, as determined by equating the nondimensional spanwise distance parameters for the two cases:

$$(z_f/\delta_{0f})Re_{\delta_{0f}}^{0.4} = (z_p/\delta_{0p})Re_{\delta_{0p}}^{0.4} \tag{3}$$

Having chosen the floor survey plane at $z_f = 8.89$ cm due to mechanical constraints, the resulting plate survey plane occurred at $z_p = 4.42$ cm according to Eq. (3).

Note that the freestream Reynolds number was the same for both cases, therefore, only the difference in δ_{0f} and δ_{0p} comes into play in Eq. (3). Note also that the above choice of survey planes is not strictly necessary in a *quasiconical* interaction.

The present 24-40-deg swept corner interaction falls within the quasiconical flow regime found in Ref. 4. Thus, the flow begins with a curved "inception zone" near the model apex, followed by a conical region based upon a virtual origin slightly to the left of the true apex. Previous results[2,4-6] indicate that conical symmetry exists within this latter region in spherical coordinates. Thus, any choice of floor and plate survey planes should be comparable in such coordinates as long as both planes are chosen outside the inception zone. The nondimensional spanwise extent of the inception zone for the present study was found from surface streak traces to have a value of 1015 in terms of the parameters of Eq. (3). Both the floor and plate survey planes were well outside this region.

Table 1 Incoming boundary-layer parameters

	δ_0, cm	δ_0^*, cm	θ_0, cm	c_f	Π
Floor	1.54	0.408	0.087	0.00116	0.70
Plate	0.42	0.112	0.023	0.00145	0.62

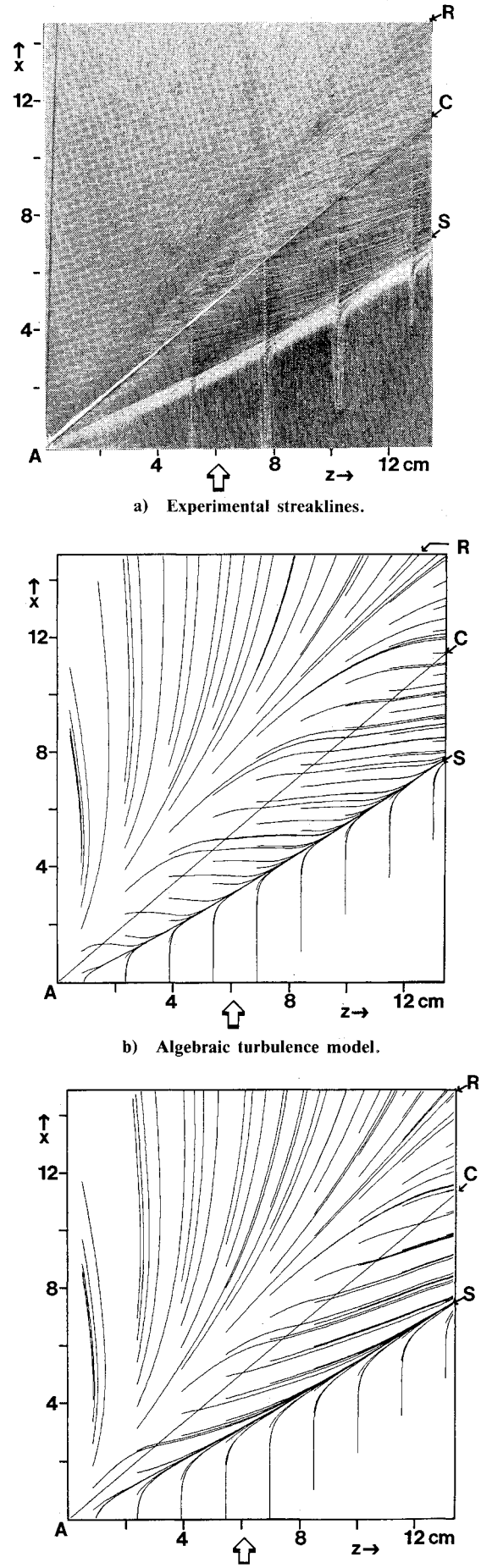

a) Experimental streaklines.

b) Algebraic turbulence model.

c) Two-equation turbulence model.

Fig. 2 Comparison of experimental and computed surface streaklines, tunnel floor.

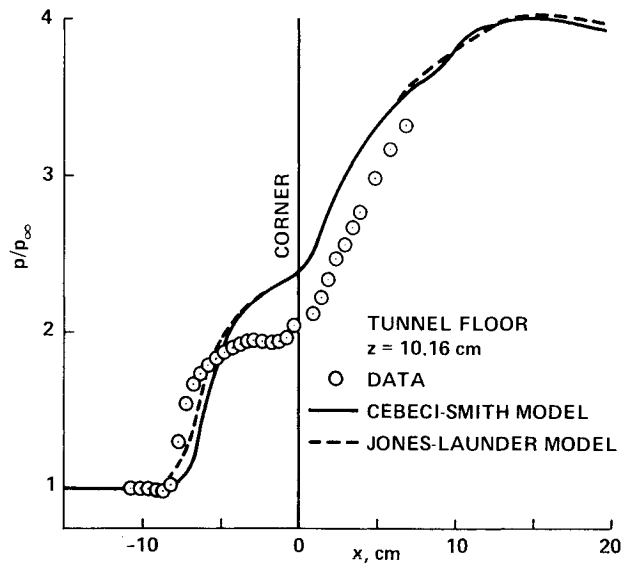

a) Tunnel floor.

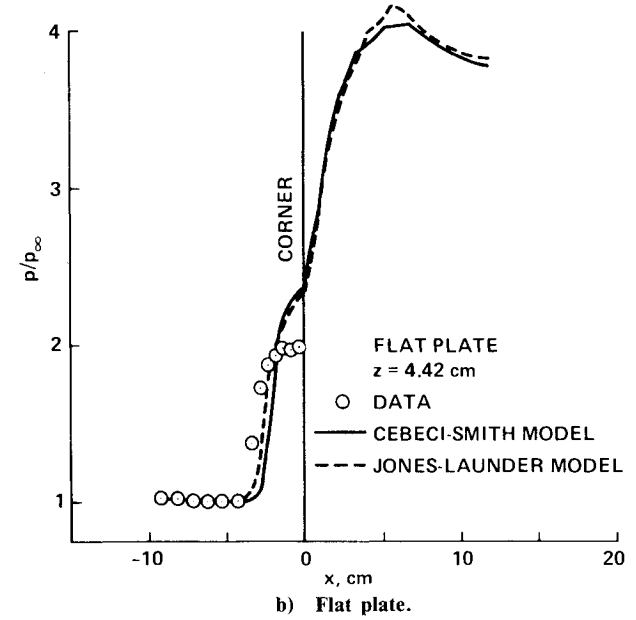

b) Flat plate.

Fig. 3 Comparison of measured and computed surface pressures.

Description of Computations

The partial differential equations used to describe the mean flowfield are the time-dependent Reynolds-averaged Navier-Stokes equations for the 3D flow of a compressible fluid. The restrictions on these equations include the perfect gas assumption, constant specific heats, Sutherland viscosity law, and zero bulk viscosity. Two eddy-viscosity models were chosen for turbulence closure: the algebraic Cebeci-Smith model[19] and the two-equation Jones-Launder model.[20] The latter requires two partial differential equations in addition to the Navier-Stokes equations. The resulting set of equations is not shown here due to space limitations, but can be found in Ref. 21.

The numerical procedure used herein is the basic explicit second-order, predictor-corrector, finite-difference, finite-volume method of MacCormack, modified by an efficient implicit algorithm.[22] The extension of MacCormack's method to three dimensions using a finite-volume concept is described by Hung and Kordulla.[11]

The computational domain extended in the streamwise direction from $5\delta_0$ upstream of the corner to $10\delta_0$ downstream, and $10\delta_0$ upward in the wall-normal direction. In the z direction the domain extended from 0 to $13\delta_0$ for the tunnel-floor case and from 0 to $18\delta_0$ for the flat-plate case. A body-fitted mesh consisting of $40\times35\times27$ points in the x, y, and z directions, respectively, allowed variable mesh-point spacing in each coordinate direction. In the x direction, the mesh spacing varied from $0.25\delta_0$ near the corner to δ_0 near the downstream boundary. In the wall-normal direction an exponentially stretched spacing near the wall was followed by a uniform spacing, yielding 20-25 mesh points within the boundary layer. The distance of the first mesh point from the wall was chosen to be small enough that the solutions were independent of the spacing, i.e., typically within

$$y^+_{\min} \equiv y(\tau_w\rho_w)^{1/2}/\mu_w < 1.0 \tag{4}$$

Finally, a uniform mesh spacing of $0.5\delta_0$ was used in the z direction.

The upstream boundary conditions were prescribed by a combination of uniform freestream conditions and the result of a boundary-layer computation along the appropriate surface (tunnel floor or flat plate). The outgoing boundary was positioned far enough downstream that all streamwise gradients could be set to zero. The no-slip condition and a constant wall temperature were applied at all test surfaces. For the Jones-Launder model the turbulent kinetic energy and dissipation rate were set to zero at the wall. Freestream conditions were applied at the upper boundary, which was sufficiently high that the shock wave exited the mesh through the rear boundary. In the cross-flow direction, symmetric conditions were applied at $z=0$ and flow quantities were extrapolated such that zero gradients existed along the corner direction at the opposite boundary.

The solution times varied from 30 to 60 min on the Cray 1S computer for the fully vectorized code, which required 800,000 words of memory. A test on c_f was used as a convergence criterion. The time required per iteration was virtually the same for the two turbulence models. (The algebraic model must determine the local boundary-layer edge and the displacement thickness at each x-z mesh point in each iteration, while the Jones-Launder model requires the solution of two additional equations.) However, due to the stiffness of the turbulence modeling equations, the maximum time step that could be used for the two-equation model was about one-half the algebraic time step. Therefore a two-equation model solution generated "from scratch" would take twice as long as an algebraic model solution. Because of the difficulties in determining an appropriate boundary-layer edge for the algebraic model in complex 3D flows, the authors believe the two-equation model is easier to use and produces more realistic solutions in this context.

Results and Discussion

Surface Properties

Figure 2a shows the kerosene-lampblack surface streak trace of the swept corner interaction on the wind-tunnel floor. Compared with this are the computed surface streaklines from the algebraic turbulence model (Fig. 2b) and the two-equation model (Fig. 2c).

The quasiconical nature of the interaction footprint (described earlier) is evident in Fig. 2. The incoming streaklines of the 2D turbulent boundary layer veer away from the streamwise direction at a line of upstream influence which becomes asymptotically conical with increasing distance from the model apex. Immediately behind the upstream influence line is a line of 3D separation toward which the streaklines converge from both sides. The inception zone to conical flow occupies roughly the left half of the interaction footprint depicted in Fig. 2. Downstream of the swept corner line there is a spreading line of flow reattachment which is also a quasiconical flow feature. A quantitative demonstration of the conical symmetry of this flow in spherical coordinates

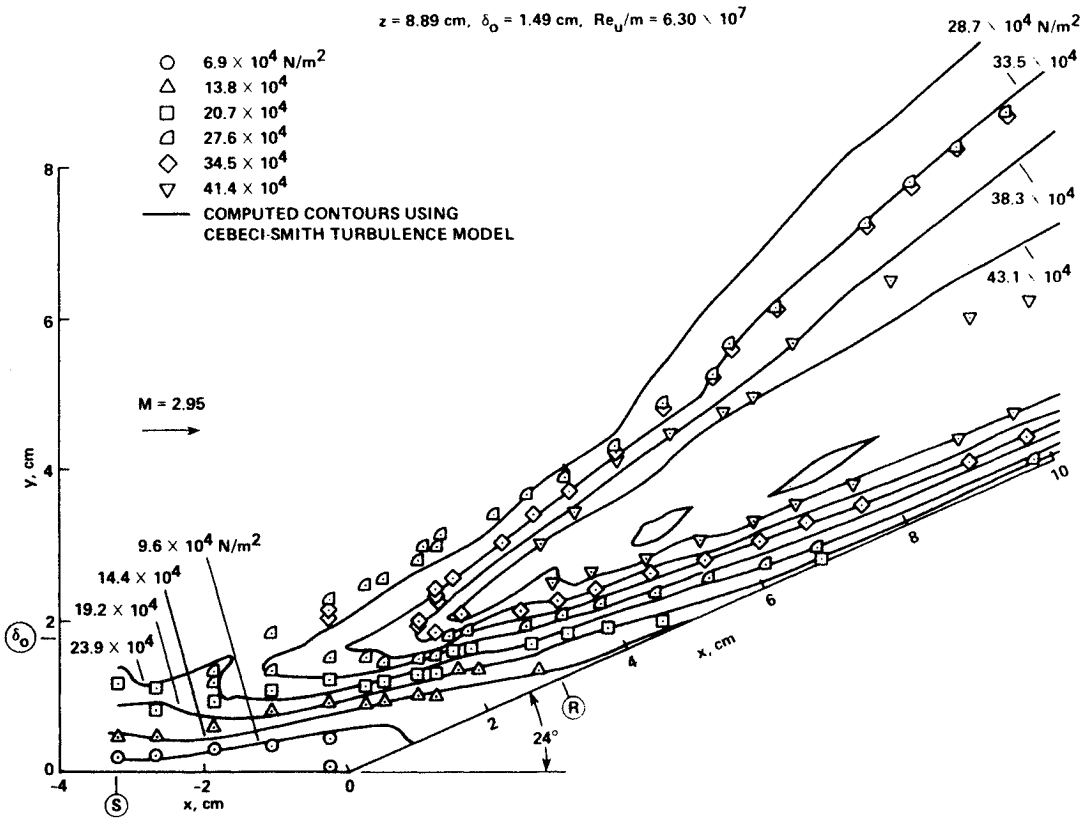

a) Algebraic turbulence model.

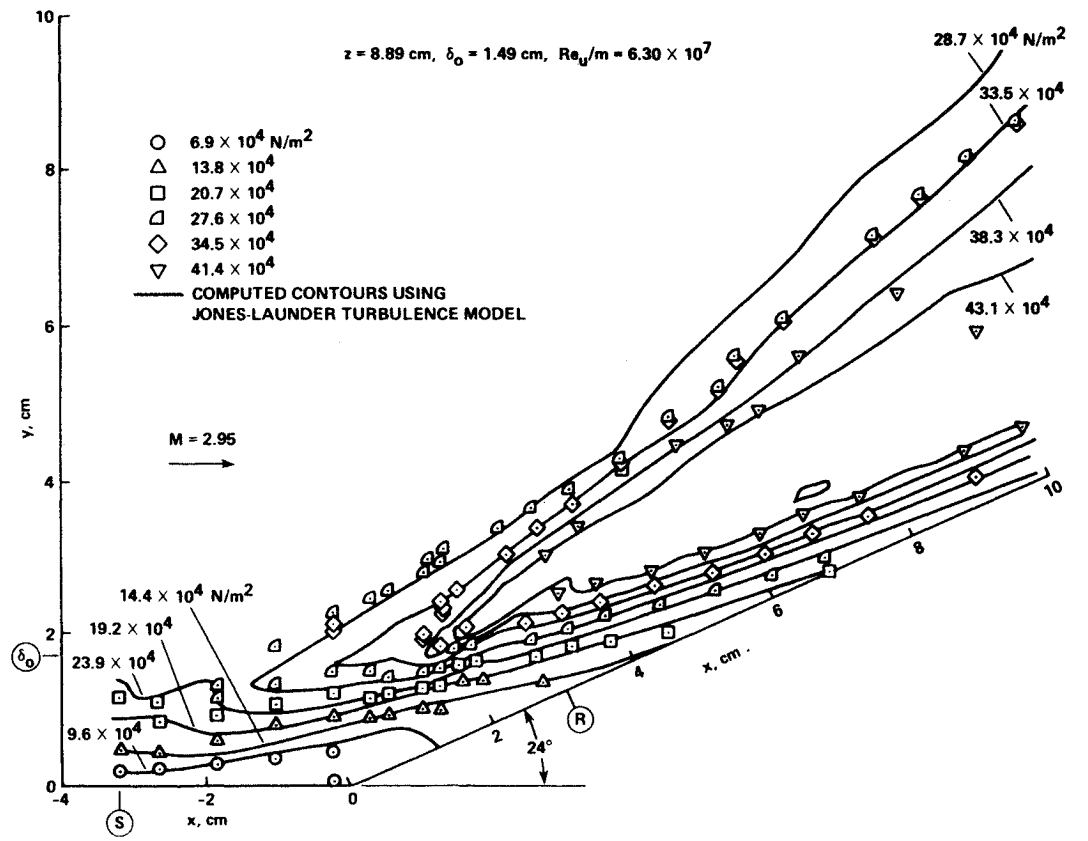

b) Two-equation turbulence model.

Fig. 4 Comparison of measured and computed pitot pressure contours, tunnel floor.

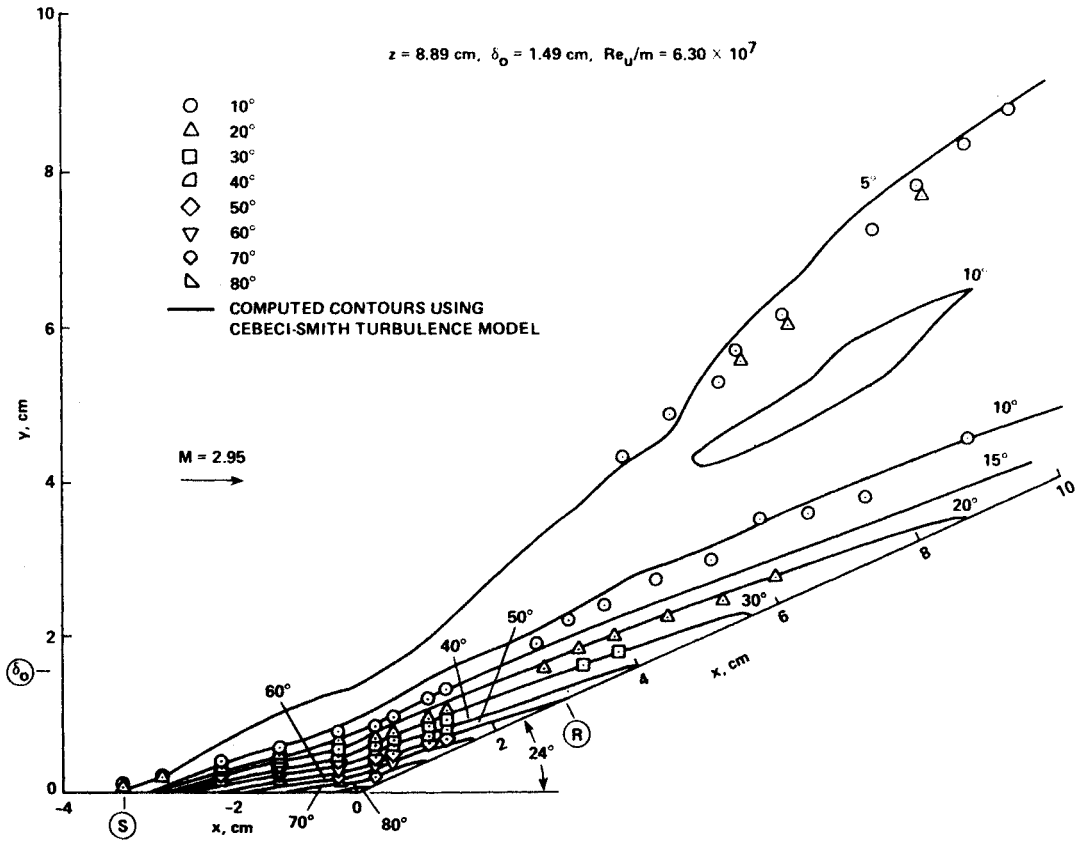

a) Algebraic turbulence model.

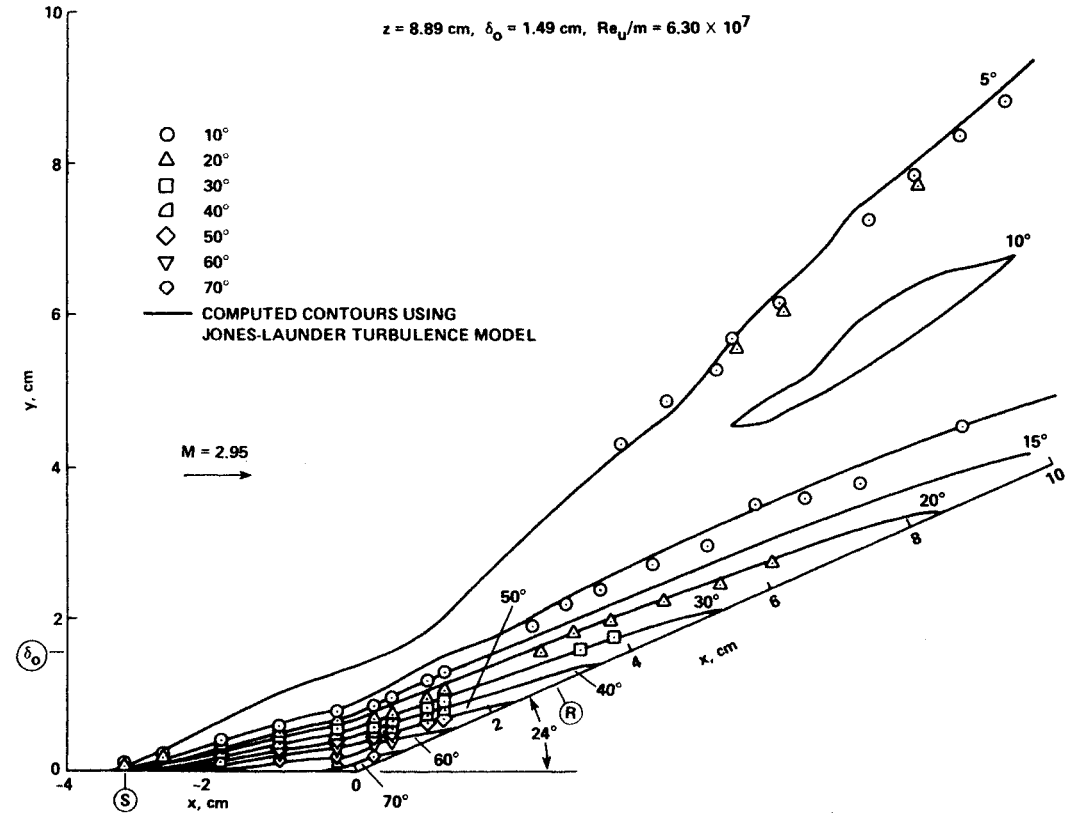

b) Two-equation turbulence model.

Fig. 5 Comparison of measured and computed yaw angle contours, tunnel floor.

outside the inception zone is omitted here due to space limitations, but is given in Refs. 4-6 and 17.

Concerning the comparison with the computed surface streamlines, Fig. 2 reveals that both turbulence model cases succeeded in predicting at least the qualitative features of the interaction footprint. However, on close inspection note that serious discrepancies occur in the immediate vicinity of the upstream influence and separation lines, where both computations underpredict the forward influence of the interaction. Further, the streak angles inside the separated flow region are accurately predicted by the two-equation computation but are in error by up to 20 deg or more in the algebraic computation. The results are substantially the same for the streakline comparison with the computations in the flat plate case (not shown here).

The measured surface pressures at selected tap rows on the tunnel floor and flat plate, along with the corresponding computed results, are shown in Fig. 3. There are only slight differences in the computed results in both cases, with the two-equation model holding a slight advantage in predicting the forward propagation of the swept corner interaction. Nonetheless, both computations significantly underpredict the forward propagation, and even more seriously overpredict the pressure level in the vicinity of the corner line ($x=0$). The slight dip in measured pressure just ahead of the corner is not predicted at all. These symptoms are the same as those observed in several past computational attempts to predict two-dimensional compression corner interactions.[23,24]

Comparisons between the experimental and computed pressure distributions for other tap rows on the floor and plate gave results similar to those shown in Fig. 3. In Fig. 3b, the pressure row chosen for the comparison had no corresponding taps on the model, therefore, no data are shown downstream of the corner.

Flowfield Properties

The results of the 26 discrete surveys carried out in the tunnel-floor interaction are best presented in the form of contour maps of pitot pressure and yaw angle (Figs. 4 and 5). Twenty-two surveys were also carried out in the flat-plate interaction but are not shown in this form, since the smaller dimensional scale of the plate interaction rendered its results less detailed.

Figures 4a and 4b show contour plots of the measured pitot pressures in the floor interaction and the results of the algebraic and two-equation Navier-Stokes computations, respectively. For clarity, the measurements are represented by discrete points, while the computations are shown by solid lines. In short, the results of the two computations are virtually identical, thus there is no indication that one outperforms the other in this context. Further, both computations appear qualitatively correct in that there is no gross mismatch with the data. Many examples of local mismatch can be found in the vicinity of the corner, where viscous effects are expected to be strongest. However, the match of data and computations in the outgoing boundary layer is impressive and probably within the interpolation error band of the comparison. Note that the computational shock smearing over at least two mesh points (3 cm) is quite obvious in Fig. 4. The outer shock was resolved to within 0.05 cm in the experimental flow surveys.

Figure 4 also reveals several interesting general features of the swept corner flowfield. The pitot contours of the boundary layer may be traced through the interaction, revealing that the boundary layer becomes a free shear layer for a short distance above the immediate corner region. The separation zone beneath this shear layer has, as expected, an almost constant pitot pressure. An initial compression (separation shock) emanates from the beginning of the interaction, followed by a second compression beginning just aft of the corner. These compressions coalesce to form the outer shock wave. More evidence of these features will be given subsequently.

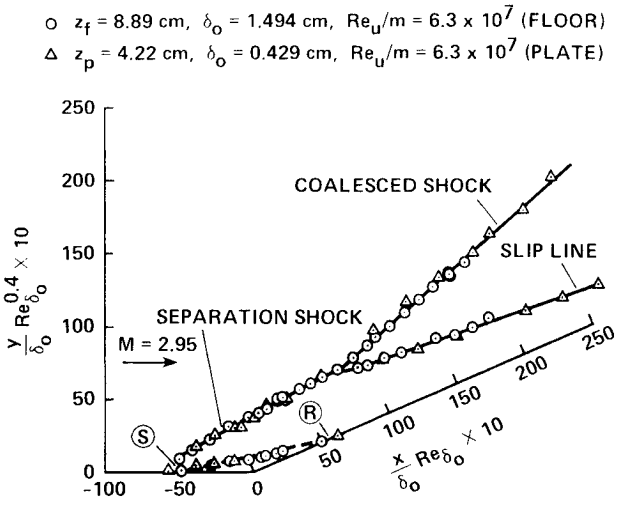

Fig. 6 Reynolds number scaling of floor and plate interaction structure.

Figure 5 shows a similar comparison of measured and computed yaw angles in the tunnel-floor interaction flowfield. Again the algebraic and two-equation results are virtually identical. The match between data and computations is generally quite good. The yaw angles between the shock system and the boundary-layer edge are small, and a progressive yawing of the flow occurs within the boundary layer as the wall is approached. The yaw angles within the separated region near the corner reach values greater than 80 deg. Though not shown here, excellent agreement was noted[17] between the measured yaw angles near the wall and the surface streakline angles shown in Fig. 2.

Flowfield Scaling

The goal of dual flow surveys with the same swept corner mounted on both the tunnel floor and flat plate is to check the ability of the established Reynolds number similarity law [Eq. (1)] to achieve an interaction flowfield as well as footprint scaling. Equation (1) is formulated in terms of x and z for footprint scaling. By replacing z with y and comparing the floor and plate interaction flowfield structures in the resulting nondimensional coordinates, this goal can be met.

Such a comparison is shown in Fig. 6. For clarity, only four main interaction features are shown: the separation shock, separation-reattachment streamline, outer (coalesced) shock, and the slip line emanating from the point of coalescence. In short, the agreement between the floor and plate results in scaled coordinates is excellent. The applicability of Eq. (1) to the Reynolds number scaling of the entire 3D interaction flowfield is thus supported.

The extent to which the computations predict this observed similarity behavior is obviously of interest. The computational shock smearing mentioned earlier confuses any comparison in the coordinates of Fig. 6. However, by returning to the interaction footprint a suitable comparison can be made. Figure 7 shows the measured and computed upstream influence line of the present swept corner interaction in the coordinates of Eq. (1). Tunnel-floor and plate data and computations are shown, although the latter represent only the Jones-Launder turbulence model, since that case was shown to have a slight advantage in predicting the upstream influence in Fig. 3. The floor and plate data are properly scaled in Fig. 7. The floor computation is in reasonable agreement with the data, although it tends to slightly underpredict the conical asymptote of the upstream influence. The fact that the plate computation appears in more serious disagreement with the data may be spurious, since the computation may not have extended far enough in the z direction beyond the inception zone leading to conically symmetric

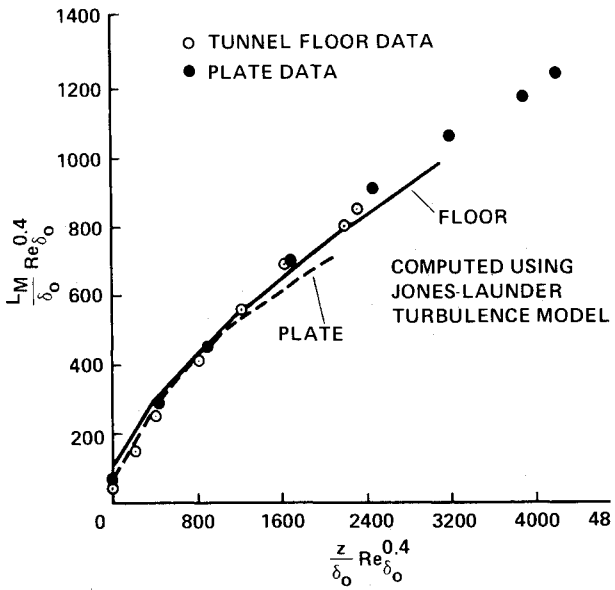

Fig. 7 Reynolds number scaling of measured and computed upstream influence lines.

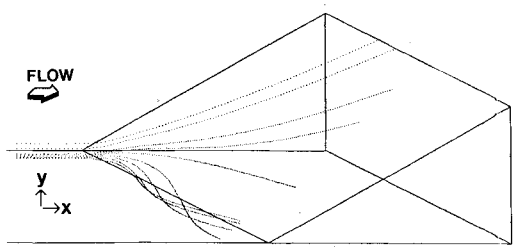

Fig. 8 Computed particle-path flow visualization.

flow. The extrapolated boundary conditions applied at the spanwise boundary of the computational domain may influence the result. Thus, although the evidence is not totally conclusive, there is at least an indication that the observed Reynolds number similarity of 3D interactions [Eq. (1)] is predicted by the present Navier-Stokes solutions. Note that a similar conclusion was reached for 2D interactions in Ref. 23.

Flow Visualization

Figure 8 shows a computed visualization of mean "particle" pathlines originating in an x-y plane near the model apex in the incoming boundary layer. The view is in the $-z$ direction from an angle of about 30 deg above the horizontal. The four particle pathlines nearest the wall are drawn into the separated flow, where they follow a helical vortex motion which is clockwise with respect to the observer. The pathlines at higher levels in the incoming boundary layer avoid the separation zone and are yawed across the model and thence swept downstream. Such a clear visualization of the motion within the separated region was not possible experimentally,[21] since it was masked by the high turbulence level. To the extent that the computation is accurate, the authors believe that this is a good example of how computations and experiments can complement one another to gain a better understanding of complex flows.

Conclusions

An experimental and computational study of the three-dimensional shock-wave/turbulent boundary-layer interaction generated by a swept compression corner has been carried out. The freestream Mach number was 2.95. Flowfield surveys were conducted with two incoming boundary-layer thicknesses varying by 3:1. These flows were predicted for the same test conditions by solutions of the Navier-Stokes equations using both algebraic and two-equation turbulence models. The goals of this study included a test of an established three-dimensional Reynolds number similarity law, the evaluation of the performance of the computations against the experimental data, and the gaining of a better physical understanding of the flow phenomenon. The general results are as follows:

1) The three-dimensional similarity law for Reynolds number effects, previously established for interaction "footprints," appears equally valid for the present *flowfield*, as indicated in Fig. 6.

2) The computed results using both turbulence models captured at least the qualitative essence of the flow. On a quantitative basis, however, several measured features of the flow were poorly predicted.

3) Computations with the more complex two-equation turbulence model held a slight advantage over those with the algebraic model.

Acknowledgments

This study was carried out under AFOSR Contract F49620-81-K-0018 with Princeton University and a related subcontract with Pennsylvania State University, monitored by Dr. James D. Wilson. The computational part of the study was funded by and carried out at NASA Ames Research Center. Discussions with Profs. D. S. Dolling and S. M. Bogdonoff are gratefully acknowledged.

References

[1]Green, J. E., "Interaction Between Shock Waves and Boundary Layers," *Progress in Aerospace Sciences*, Vol. 11, 1970, Pergamon Press, New York, pp. 235-340.

[2]Settles, G. S. and Dolling, D. S., "Swept Shock Wave-Boundary Layer Interactions," *Missile Aerodynamics, AIAA Progress in Astronautics and Aeronautics*, to be published.

[3]Settles, G. S. and Bogdonoff, S. M., "Scaling of Two- and Three-Dimensional Shock/Turbulent Boundary-Layer Interactions at Compression Corners," *AIAA Journal*, Vol. 20, June 1982, pp. 782-789.

[4]Teng, H-Y. and Settles, G. S., "Cylindrical and Conical Flow Regimes of Three-Dimensional Shock-Wave/Turbulent Boundary-Layer Interactions," *AIAA Journal*, Vol. 22, Feb. 1984, pp. 194-200.

[5]Settles, G. S. and Lu, F. K., "Conical Similarity of Shock/Boundary-Layer Interactions Generated by Swept and Unswept Fins," *AIAA Journal*, Vol. 23, July 1985, pp. 1021-1027.

[6]McClure, W. B. and Dolling, D. S., "Flowfield Scaling in Sharp Fin-Induced Shock Wave Turbulent Boundary Layer Interaction," AIAA Paper 83-1754, July 1983.

[7]Horstman, C. C. and Hung, C. M., "Computation of Three-Dimensional Turbulent Separated Flows at Supersonic Speeds," AIAA Paper 79-0002, Jan. 1979.

[8]Knight, D. D., "A Hybrid Explicit-Implicit Algorithm for the Three-Dimensional Compressible Navier-Stokes Equations," AIAA Paper 83-0223, Jan. 1983.

[9]Kussoy, M. I., Viegas, J. R., and Horstman, C. C., "An Experimental and Numerical Investigation of a 3D Shock Separated Turbulent Boundary-Layer," AIAA Paper 80-0002, Jan. 1980.

[10]Horstman, C. C., "A Computational Study of Complex Three-Dimensional Compressible Turbulent Flow Fields," *AIAA Journal*, Vol. 23, Oct. 1985, pp. 1461-1462.

[11]Hung, C. M. and Kordulla, W., "A Time-Split Finite-Volume Algorithm for Three-Dimensional Flowfield Simulation," AIAA Paper 83-1957, July 1983.

[12]Viegas, J. R. and Horstman, C. C., *Proceedings of 1980-81 AFOSR-HTTM-Stanford Conference on Complex Turbulent Flows*, Vol. III, edited by S. J. Kline, B. J. Cantwell, and G. M. Lilley, Stanford Univ., Stanford, CA, 1981, pp. 1535-1539.

[13]Settles, G. S. and Perkins, J. J., "Investigation of Three-Dimensional Shock/Boundary Layer Interactions at Swept Compression Corners," AIAA Paper 79-1498, July 1979.

[14]Settles, G. S. and Teng, H-Y., "Flow Visualization Methods for Separated Three-Dimensional Shock-Wave/Turbulent Boundary

Layer Interactions," *AIAA Journal*, Vol. 21, March 1983, pp. 390-397.

[15]Settles, G. S. and Teng, H-Y., "A Test of the Independence Principle in Swept Cylindrical Shock Wave/Turbulent Boundary Layer Interactions," Paper B-4.2, presented at the 2nd Asian Congress of Fluid Mechanics, Beijing, China, Oct. 1983.

[16]Settles, G. S. and Kimmel, R. L., "Similarity of Quasiconical Shock Wave/Turbulent Boundary Layer Interactions," *AIAA Journal*, Vol. 24, Jan. 1986, pp. 47-53.

[17]McKenzie, T. M., "A Flowfield Scaling of Three-Dimensional Shock/Boundary Layer Interaction of the Swept Compression Corner," M.S. Thesis 1598-T, Mechanical and Aerospace Engineering Department, Princeton University, Princeton, NJ, June 1983.

[18]Mathews, D. C., Childs, M. E., and Paynter, G. C., "Use of Coles' Universal Wake Function for Compressible Turbulent Boundary Layers," *Journal of Aircraft*, Vol. 7, March-April 1970, pp. 137-140.

[19]Cebeci, T. and Smith, A. M. O., *Anaylsis of Turbulent Boundary Layers*, Academic Press, New York, 1974.

[20]Jones, W. P. and Launder, B. E., "The Prediction of Laminarization with a Two-Equation Model of Turbulence," *International Journal of Heat and Mass Transfer*, Vol. 15, Feb. 1972, pp. 301-314.

[21]Settles, G. S., Horstman, C. C., and McKenzie, T. M., "Flowfield Scaling of a Swept Compression Corner Interaction—A Comparison of Experiment and Computation," AIAA Paper 84-0096, Jan. 1984.

[22]MacCormack, R. W., "A Numerical Method for Solving the Equations of Compressible Viscous Flow," *AIAA Journal*, Vol. 20, Sept. 1982, pp. 1275-1281.

[23]Horstman, C. C., Settles, G. S., Vas, I. E., Bogdonoff, S. M., and Hung, C. M., "Reynolds Number Effects on Shock-Wave Turbulent Boundary-Layer Interactions," *AIAA Journal*, Vol. 15, Aug. 1977, pp. 1152-1158.

[24]Visbal, M. R. and Knight, D. D., "Evaluation of the Baldwin-Lomax Turbulence Model for Two-Dimensional Shock Wave Boundary Layer Interactions," AIAA Paper 83-1697, July 1983.